Available online at www.sciencedirect.com
ScienceDirect
International Journal of Solids and Structures 43 (2006) 7752–7775
INTERNATIONAL JOURNAL OF SOLIDS and STRUCTURES
www.elsevier.com/locate/ijsolstr

A study on an axial crush configuration response of thin-wall, steel box components: The quasi-static experiments

B.P. DiPaolo *, J.G. Tom

US Army Engineer Research and Development Center, Vicksburg, MS 39180, USA

Received 5 January 2006; received in revised form 20 March 2006
Available online 7 April 2006

Abstract

An experimental investigation was performed to study a specific axial crush configuration response of steel, square box components under quasi-static testing conditions. For a specific cross-sectional geometry/fabrication process, test specimens were obtained from commercially produced, welded tube lengths of ASTM A36 and ASTM A513 Type 1 plain low-carbon steels and AISI 316 and AISI 304 austenitic stainless steels. Removable grooved caps were used to constrain tube test specimen ends, and collapse initiators in the form of shallow machined grooves were used to control the initial transverse deformations of the test specimen sidewalls. The progressive plastic deformation for all of the test specimens was restricted to the prototype configuration response (fold formation process and the corresponding axial load-axial displacement curve shape) of the symmetric axial crush mode. Crush characteristics were evaluated and, for each material type, observed differences were less than 7% for maximum and minimum load magnitudes and less than 2% for energy absorption, displacement, and mean load quantities in both the initial phase and the secondary folding phase cycles. Overall, results of the study indicate that for a significant range of material strengths, a controlled and repeatable energy absorption process can be obtained for commercially produced steel box components undergoing symmetric axial crush response. Published by Elsevier Ltd.

Keywords: Axial crush; Configuration response; Thin-wall box components; Steel; Progressive collapse; Plastic deformation; Energy absorption; Quasi-static experiments

1. Introduction

Axial crush response of thin-wall, ductile metallic alloy components (specific geometry and material combination) has been extensively studied for irreversible directional energy absorption capability (Coppa, 1968; Ezra and Fay, 1972; Johnson and Reid, 1978; Reid and Reddy, 1986; see overview of dynamic progressive buckling in Jones, 1997). Because significant energy can be absorbed by plastic deformation during the progressive fold formation process that is characteristic of this response, axial crush has many important engineering safety applications in areas including crashworthiness and blast-resistant design of structures.

* Corresponding author. Tel.: +1 601 634 4021; fax: +1 601 634 2309.
E-mail address: Beverly.P.DiPaolo@erdc.usace.army.mil (B.P. DiPaolo).

0020-7683/$ - see front matter Published by Elsevier Ltd.
doi:10.1016/j.ijsolstr.2006.03.028

An example of the symmetric axial crush response mode (Abramowicz and Jones, 1984) for an AISI 304 stainless steel, welded square box component tube specimen is shown in Fig. 1. A crush specimen showing the fold formation is next to an undeformed tube specimen in Fig. 1a and, the corresponding axial load-axial displacement curve (subsequently referred to as the load–displacement curve) is shown in Fig. 1b and c. Axial crush response can be considered to consist of phases or stages (Pugsley, 1960). For the current investigation, the type of response shown in Fig. 1 is divided into an "initial" phase and a "secondary" phase. The initial phase includes the pre-collapse response prior to the occurrence of the peak or maximum load, the change from axial to bending load-resistance in the sidewalls, and the formation of the first few interior and exterior folds on sets of opposite sidewalls with corresponding increases and decreases in the load–displacement curve. The secondary folding phase consists of the "steady state" fold formation process. In this phase, adjacent sidewall interactions and contacting of folds produce subsequent fold formations of constant wavelength along the remaining length of the specimen. For the current investigation, a cycle in the curve (see Fig. 1b) corresponds to the formation of one exterior or one interior fold on both sets of opposite sidewalls with load magnitudes fluctuating between minimum and maximum values. Cycles can be further divided into sections. Each section represents the formation of an exterior fold on a specific set of opposite sidewalls and the corresponding formation of an interior fold on the other opposite sidewall pair.

For axial crush response, investigators have used or defined "crush characteristics", also called indicators or parameters, to evaluate and compare the performance of components (Pugsley, 1960; Coppa, 1968; Magee and Thornton, 1979). These characteristics include both direct data and derived quantities. The emphasis of the current investigation is on the direct data quantities from the load–displacement curve. These characteristics of interest are shown in Fig. 1c for the square box component and include: the initial phase peak load, $P_{\max}$ (or P_{02}); maximum and minimum loads, P_{ij}; mean or average loads, $P_{\text{mean}i}$; energy absorptions, EA_i; and axial displacements, δ_i. The subscript i refers to the initial phase if $i = 0$ and the ith cycle in the secondary

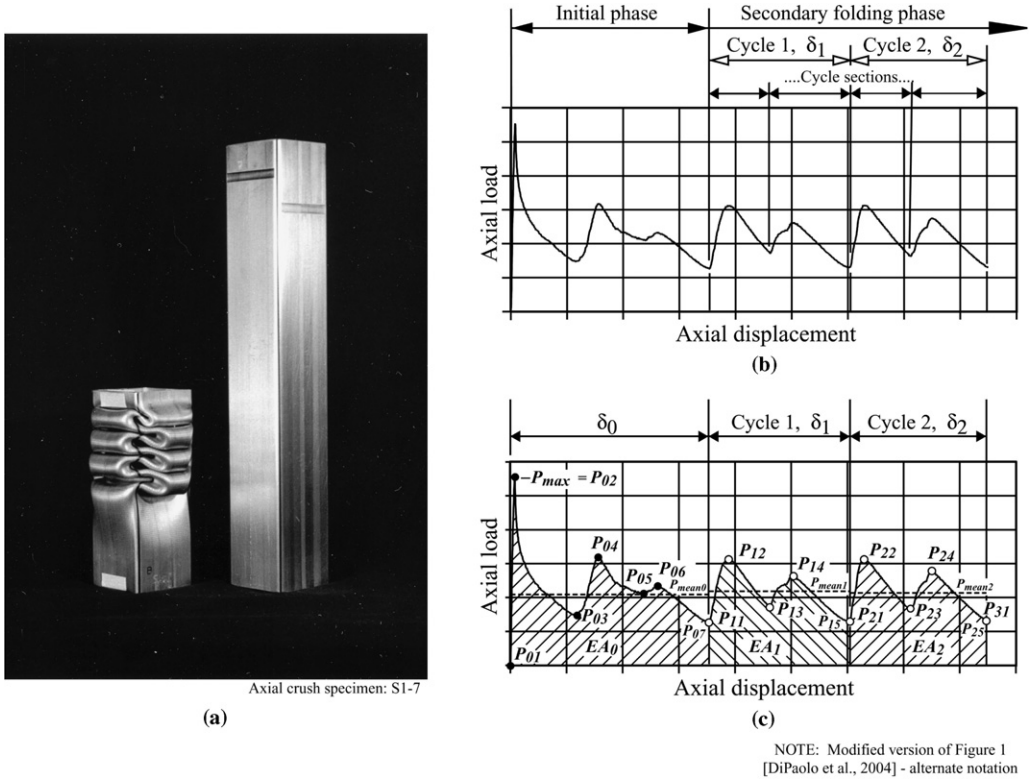

Fig. 1. Symmetric axial crush response mode – ductile metalic alloy, square box component: (a) axial crush and undeformed tube specimens, (b) curve sections and (c) crush characteristics.

phase for $i = 1, 2$, etc. The subscript j is a sequential number indicator for the maximum and minimum loads in the initial phase or in an ith cycle. In general, an energy absorption quantity, EA_i, is the area under the load–displacement curve, and $P_{\text{mean}i}$ is equal to the energy absorption divided by the axial displacement, δ_i for the initial phase or the ith cycle.

In general, axial crush response has been investigated with respect to types of response modes (Abramowicz and Jones, 1984; Andrews et al., 1983), geometry-material design criteria for components (Mahmood and Paluszny, 1981, 1982), crush characteristics to evaluate performance (Coppa, 1968; Magee and Thornton, 1979), methods to initiate or modify response (Yamaya and Tani, 1971; Thornton, 1975; Mamalis et al., 1986; Lee et al., 1999), and rate and temperature effects (VanKuren and Scott, 1978). Researchers have also investigated effects of material type, material alloying, and process parameters on the axial crush response of metallic alloy components. Results have shown response mode changes from ductile fold formation to fracture (Magee and Thornton, 1979; Thornton, 1979; McGregor et al., 1993) and differences in mode response and crush characteristic magnitudes in the fold formation process (Toda et al., 1976; VanKuren and Scott, 1978; Geoffroy et al., 1993; Gupta and Gupta, 1993; Logan et al., 1993; Langseth and Hopperstad, 1996; Seitzberger et al., 2000). However, analyses involved peak load and overall crush displacement and energy absorption quantities. Secondary folding phase characteristics and details of the materials undergoing severe plastic deformation could not be evaluated because of significant differences in the fold formation process and the load–displacement curve shapes for specimens within each individual research study.

The term "configuration response" was introduced in past research involving AISI 304 stainless steel square box components (DiPaolo et al., 2004). For the symmetric axial crush mode, a specific "configuration response" refers to the combination of a specific fold formation process (verified by fold appearance) and the shape of the corresponding load–displacement curve. An example of fold formation and the corresponding load–displacement curve of an AISI 304 stainless steel tube specimen for the "Configuration A" response that was studied in the previous research is given in Fig. 2. The results of the past research showed that, for specimens of a given component (constant geometry and material), there were several configuration responses of the symmetric axial crush mode and that these configuration responses differed in stationary foldline locations and traveling foldline paths (for concepts of stationary and traveling foldlines of hat-section specimens, see Ohkubo et al., 1974, and for right-circular cylindrical polyvinyl chloride specimens, see Soden et al., 1974; for idealized models, plastic "hinge lines", see Ohkubo et al., 1974, and for right-circular cylindrical and square specimens, see Johnson et al., 1977; Abramowicz and Wierzbicki, 1979) and, therefore, differed in load magnitudes, energy absorption processes and material performance requirements. It was demonstrated that axial crush response could be controlled and restricted to a specific configuration response for tube specimens with constant geometry and material and, also, for tube specimens with constant geometry and of the same alloy, but having different uniaxial tensile strength levels. This capability is important not only for the practical application of axial crush response, but also because it provides the ability to research the influence of material

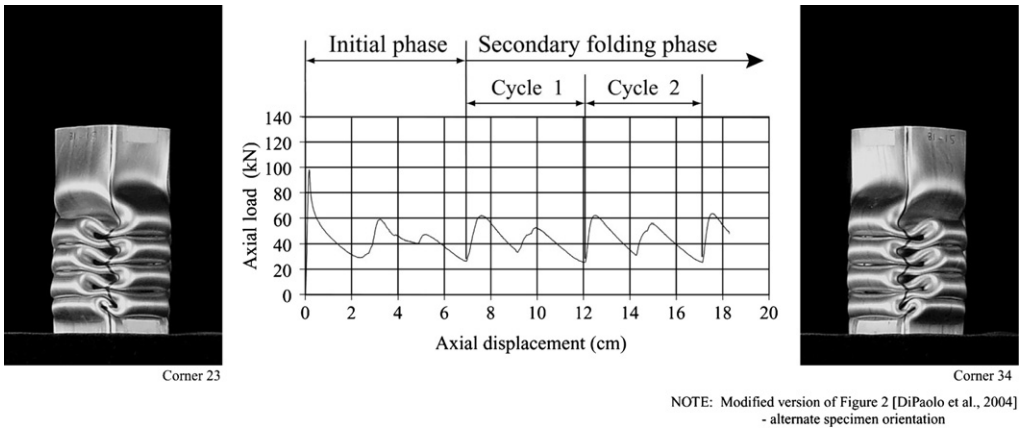

Fig. 2. Configuration A response – prototype specimen S1-18: fold formation and load–displacement curve.

parameters on axial crush characteristic magnitudes and to study details of material behavior such as microstructural evolution and deformation mechanisms during severe plastic deformation.

The current experimental investigation is an extension of this previous research. The first objective was to demonstrate the ability to consistently obtain the same symmetric axial crush mode configuration response for commercially produced, welded square box component specimens of several steel materials in a single geometry. The second objective was to examine the effect of material parameters on the fold formation process and crush characteristics for the specific configuration response induced in the components.

2. Experimental methodology

The experimental study was based on quasi-static axial crush to minimize inertial, strain rate, and heat-of-deformation effects. The test specimens consisted of thin-wall, steel square box components in material-geometry combinations that theoretically have the ability to undergo symmetric axial crush response and are applicable to vehicular crash and blast-protective applications.

2.1. Box component specimens

The tube specimens were fabricated from commercially produced, welded tube lengths with a square cross-sectional geometry. The tubing was purchased "off-the-shelf" from the regular stock of commercial metallic alloy product suppliers. The cross-section geometry was set to a "constant" 50 mm × 50 mm square outside dimension and a nominal 16-gage wall thickness for all tube lengths.

2.1.1. Materials

Steel materials were used in the investigation because they are widely produced, commonly used, and have been extensively researched. Steel materials are known for excellent mechanical properties with respect to strength, ductility, and toughness. Specifically, the steel alloys used were selected to study the effect of strength level, strain-hardening characteristics, and ductility and microstructural deformation mechanisms in the plastic fold formation process of axial crush response. The steel materials are:

- Structural ASTM A36 (A36) plain low-carbon steel,
- Mechanical ASTM A513 Type 1 (A513) plain low-carbon steel,
- AISI 316 (316SS) wrought austenitic stainless steel,
- AISI 304 (304SS) wrought austenitic stainless steel.

The ASTM A36 material in square tube length product forms (ASTM A36-05, ASTM A500-03a) is plain, low-carbon steel and has been referred to as "mild steel". In the 16-gage thickness, the steel is hot-rolled. The ASTM A513 Type 1 ERW (electric resistance welded) mechanical tubing material is also a plain, low-carbon (specified as AISI 1008/1015; O'Neal, 2002b) hot-rolled steel (ASTM A513-00).

The AISI 316 stainless steel material is a highly corrosion resistant, molybdenum-bearing, wrought austenitic stainless steel. Chemical composition requirements (ASTM A666-03) include 16.0–18.0% chromium and 10–14% nickel. The chromium is the principal element affecting the corrosion resistance and stabilizes delta-ferrite; whereas, the nickel stabilizes austenite. AISI 316 stainless steel is considered "stable" because the austenite does not readily transform to martensite during plastic straining at and around 20 °C (room temperature) (Maldonado et al., 1994).

The AISI 304 stainless steel material for mill-surface finish, ornamental/structural grade tubing (Ryerson, 1991) is also highly corrosion resistant but is a basic "18–8" wrought austenitic stainless steel that is alloyed with 18.0–20.0% chromium and 8–10.5% nickel (ASTM A666-03). The 304SS material is considered "metastable" because it may have the ability to undergo a strain-induced transformation of austenite to martensite when subjected to severe plastic deformation at and around 20 °C (Angel, 1954; Griffiths and Wright, 1969). If the transformation occurs, the strength behavior, e.g., strain-hardening and stress–strain curve shape, in a given stress/strain state is primarily derived from the mechanical response of the austenite, the transformation from austenite to martensite, and the mechanical response of the product martensite. The occurrence and

degree of the transformation depend not only on the composition, grain size, grain orientation, and temperature during deformation, but also on the stress/strain state and strain magnitude, rate, and path (Gray et al., 1985; Powell et al., 1958; Hecker et al., 1982). Martensite resulting from the transformation can be a ferromagnetic body-centered cubic α' phase or a non-ferromagnetic hexagonal close-packed ε phase. In the annealed state, the 304SS material is generally nonmagnetic and therefore, after severe plastic deformation, a positive response to a small magnet would indicate that α'-martensite had formed in the area and that the martensitic transformation had occurred.

2.1.2. Tube lengths, sectioning of the tube lengths, and tube specimen numbering systems

One to four lengths of tubing were obtained for each steel material. As shown in Fig. 3a, tubing length varied from 240 cm to 625 cm and depended on availability from the supplier. Upon delivery, a full tube length was given an identification designation in the form "ID#", where "ID" represents the alloy type/supplier and for multiple lengths of the same alloy type/supplier, "#" is the number assigned that specific tube length. The exception to this designation is the A36 tubing. This tubing was purchased as a single tube length that was cut into smaller sub-lengths by the supplier to accommodate a 2.4 m shipping container length limit, and mechanical property tests were performed on specimens from each of the A36 sub-lengths to confirm consistent material strength. The alloy type/supplier ID's are given in Fig. 3b and the ID# lengths specifically used to obtain test specimens in the current investigation are

- C2 and C4 for the A36 tube length (OnlineMetals, 2002),
- M1 for the A513 tube length (O'Neal Steel, 2002b-HREW),
- T2 and X1 for the 316SS tube lengths (O'Neal Steel, 2002a-AISI316; Empire, 2003),
- S2, S3 and S4 for the 304SS tube lengths (Ryerson, 1998).

From prior axial crush testing of 304SS tube specimens of similar cross-sectional geometry to that used in the current investigation, it had been determined that a tube specimen length of 30.5 cm was adequate to obtain at least two full fold cycles in the secondary folding phase of several symmetric axial crush mode configuration responses without the tube end constraint conditions adversely affecting the secondary phase fold formation process. All tube lengths were sectioned into tube specimens using cutting sequences based on the 30.5 cm axial crush tube specimen length. Two cutting sequences were used and are shown in Fig. 3a. The first cutting sequence was for the 304SS tube lengths that had been obtained and used in previous research (DiPaolo, 2000). This sequence consisted of an initial cutting and a subsequent cutting that resulted in nineteen tube specimens of approximately 30.5 cm in length and four miscellaneous tube pieces of lengths less than 10.0 cm. The lengths of tube specimens obtained by sub-cutting are slightly less than 30.5 cm due to the saw blade thickness. The other tube lengths had been obtained for the current research and the cutting sequence used for these lengths included an initial cutting of a short piece and then uniform cutting of 30.5 cm tube specimens resulting in a last short tube piece. The number of 30.5 cm specimen lengths depended on the initial tube length.

To begin a tube length sectioning, one end was arbitrarily chosen as the "start" end for the cutting of tube specimens. All sectioning was performed using cutoff saws and at a slow speed to avoid heating in the material. Cutting lines were made as perpendicular as possible to the longitudinal axis of the tube length. All tube specimen ends were deburred, but not milled.

A specimen numbering system was used to track the original tube length location for a tube specimen or piece and is shown in Fig. 3a. The specimen number was of the form ID#-initial tube length cut number (– cut-sub-number, if applicable). The number was engraved at two specific locations on the tube specimen or piece in a specified orientation to track the cutting direction and establish the sidewall and corner numbering system shown in Fig. 3c and d. This specimen numbering system is used to locate and identify corners and to orient any material point on a specimen along the original tube length and around the tube cross-section.

2.1.3. Geometry

2.1.3.1. Cross-section attributes. For one specimen from each tube length, the end-of-cutting end was wet ground perpendicular to the longitudinal tube length axis. The ID#-1 specimens were used for the

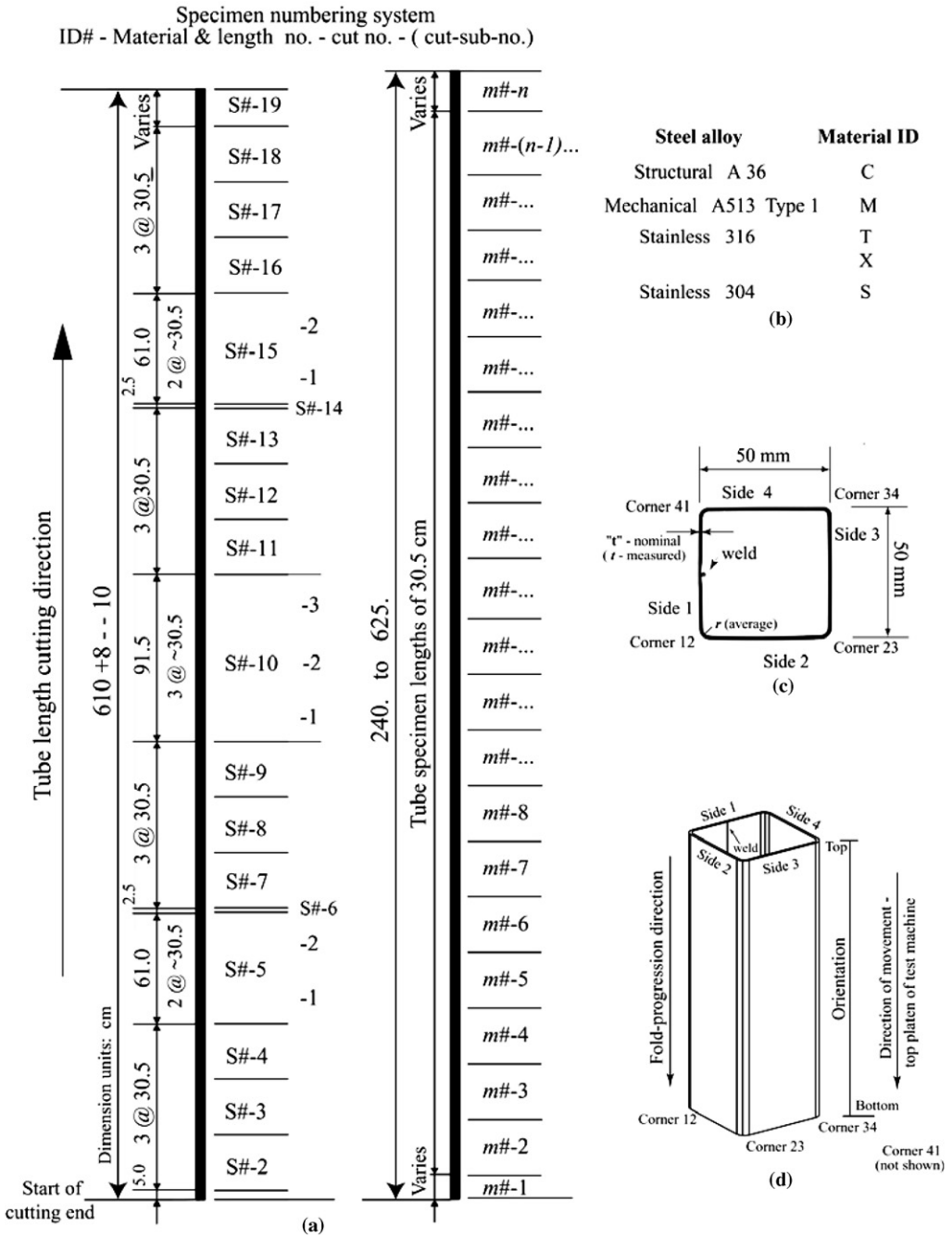

Fig. 3. Commercially produced, welded square box cross-section tube lengths: (a) length cutting diagrams for 304SS lengths and lengths of an arbitrary material m with n pieces, (b) materials, (c) cross-section geometry – 304SS S1 example and (d) tube specimen orientation corner numbering system.

A36-C2 and C4, A513-M1 and 316SS-X1 tube lengths and, for the 304SS tube lengths, the specimens used were S1-8, S2-9, S3-8 and S4-8. Grinding was performed using glass plates and silicon carbide metallographic grinding papers in the grit sequence of 80, 240, 320, 600, 1200 and 4000 (Buehler, 2003; Struers, 2003). Thickness and corner radii of the tube ends were measured from images scanned from the ''polished'' cross-sections.

Visual examination and the scanned images indicated that tube lengths obtained for this study had one of two square, box cross-sectional geometries. Each geometry is a result of the fabrication method used to cold-form the square tubing. The first cross-sectional geometry with its corresponding fabrication process represents the A36-C#, A513-M#, 304SS-S#, and 316SS-X# tube length cross-sections and will be referred to as the ''geometry/fabrication-1'' type. Relatively large radius, ''rounded'' corners and slight outwardly curved sidewalls characterize this cross-section geometry. The tube lengths with this cross-sectional geometry were formed from welded circular tubing by processes such as shaping passes by sets of rollers or die forming on sidewall regions. Examples of this geometry/fabrication type are shown in Fig. 3c for the 304SS S1-8 tube specimen and in Fig. 4a for the 316SS X1-1 tube specimen. Fig. 4b shows an example of the ''geometry/fabrication-2'' cross-section that is characteristic of the 316SS-T# tube lengths. The cross-section geometry has relatively small radius, ''tightly'' bent corners and flat sidewalls and is the result of square tube fabrication methods involving operations such as box and pan break pressing. Deformation during forming is concentrated at and near the cornerlines.

For each geometry/fabrication type, the process to form the square tube cross-sections produces specific residual stress patterns and mechanical property variations around the tube cross-section in the material. Generally, no annealing is performed during or after fabrication for the commercial forming processes described above. To be applicable for axial crush applications, a fabricated, square-tube component (specific geometry and material combination) has to have the ability to undergo the severe plastic deformation stress/strain paths required by axial crush without material failure such as cracking that would interfere with the fold formation process. Previous research (DiPaolo, 2000) has indicated that the 304SS tube specimens with their geometry/fabrication-1 cross-section could undergo axial crush response without material failure. However, no testing had been performed for either geometry/fabrication type for the other steel materials.

Both the geometry/fabrication-1 and the geometry/fabrication-2 cross-sections were obtained for the 316SS material and the corresponding tube lengths were X1 and T2, respectively. Several tube specimens were quasi-statically axially compressed from both lengths. For the X1 specimens, the progressive fold formation process was typical of the symmetric axial crush mode response and no material failure occurred. An example of the fold formation is shown in Fig. 4a for specimen X1-7. However, for the T2 specimens, although fold formation progressed down the longitudinal axis of the specimens, extensive cracking occurred along the C23 and C34 cornerlines that are opposite the sidewall containing the longitudinal weld. An example of this cracking in the fold formation on Corner 23 of specimen T2-15 is shown in Fig. 4b. As results of uniaxial tension testing of mid-sidewall side 3 specimens from tube specimens T2-3 and X1-3 indicated similar levels of strength and

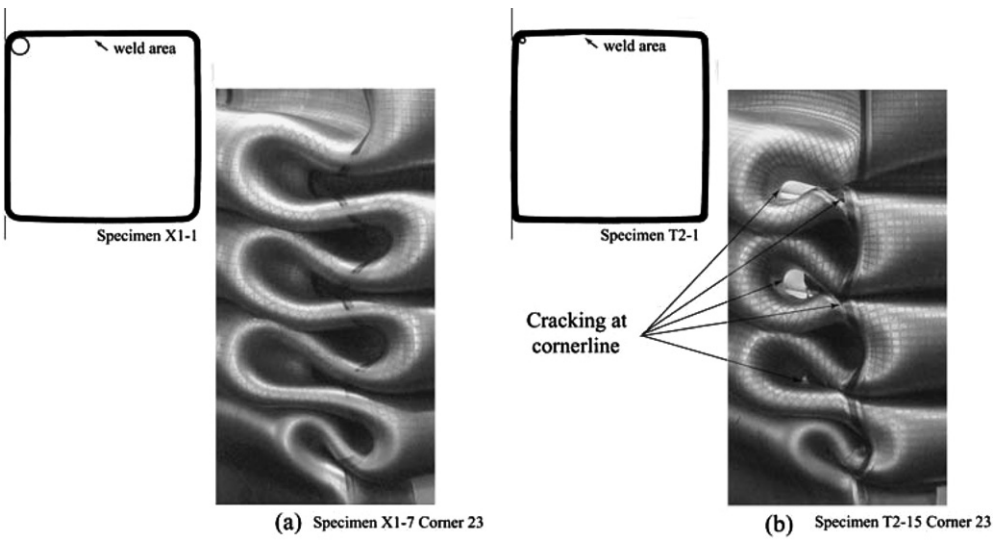

Fig. 4. Geometry and fold formation response differences for 316SS tube lengths: (a) tube length X1 specimen and (b) tube length T2 specimen.

ductility, the T2 cornerline cracking was attributed to reduced material deformation capability resulting from the geometry/fabrication-2 square tube forming process.

The testing of both geometry/fabrication cross-section types in the same material alloy indicates that the ability of a component to undergo axial crush depends not only on overall geometry and material parameters, but also on local material conditions resulting from the fabrication process. Because of the consistent occurrence of the corner cracking, the T2 tube specimens were excluded from the study, and only specimens from the X1 tube length represented the 316SS material. As a result, the remainder of the study includes only the tube lengths with the geometry/fabrication-1 cross-section.

2.1.3.2. Wall thickness. For all ID# lengths that were used in the investigation, wall thickness on all four sides was measured for every tube specimen. The average mid-sidewall thickness values are given in Fig. 5. The values deviate from the nominal standard 16-gage thickness of 1.52 mm for ferrous sheet (Manufacturers' Standard) and 1.59 mm for stainless steel sheet (US Standard) (O'Neal, 2002a). The A513 M1 tube length specimens with an average wall thickness of 1.51 mm have the largest average wall thickness of all of the tube lengths. The 304SS S2, S3 and S4 tube length specimens have the same average wall thickness of 1.49 mm. The maximum percent difference based on minimum values is less than 3% for the A513 M1, 316SS X1 and 304SS S2, S3 and S4 tube lengths specimens. The A36 C2 and C4 tube length specimens with an average wall thickness of 1.40 mm have the minimum average wall thickness, and there is an 8% difference in average wall thickness between the A513 M1 and the A36 C2 and C4 specimens. For each tube specimen from a given ID# length, cross-section outline tracings of the "end-of-cutting" end were superimposed. The results indicated

							ASTM standard specification		
								Min. requirements	
Steel type	Designation (ASTM or AISI)	Specimen length-cut number	*t* Thickness (mm)	Yield stress (MPa)	Type	Ultimate strength (MPa)	Specification number	Yield stress (MPa)	Ultimate strength (MPa)
Structural	A36	C2-3	1.40	337		365	A500-03a	228	310
		C4-3	1.40	340	0.2% offset	364	Grade A round structural tubing		
Mechanical	A513 Ty 1	M1-3	1.51	400	upper yield point	448	A513-00	241	331
							1008/1015 as-welded round tubing		
Stainless	316	X1-3	1.47	468	0.2% offset	679	A666-03	205	515
							annealed condition		
Stainless	304	S2-3	1.49	380	0.2% offset	683	A666-03	205	515
		S3-3	1.49	420	0.2% offset	740	annealed condition		
		S4-3	1.49	439	0.2% offset	761			

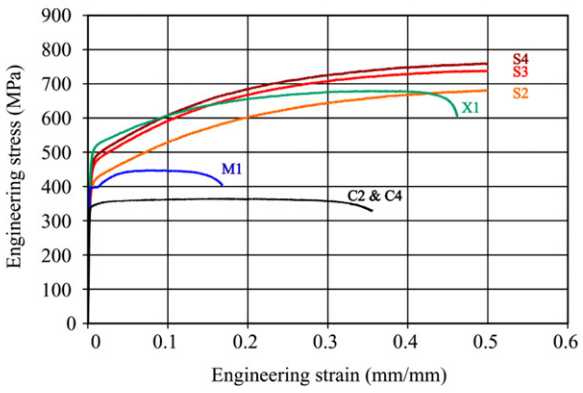

Fig. 5. Quasi-static uniaxial tension tests results.

no significant differences in outer perimeter shape and dimensions and in wall thickness for the tube specimens and, therefore, tube specimens from the same ID# length had constant geometry. For several tube specimens for a given ID# length, outer dimensions were measured and recorded. Results of the tracings, measurements, and scans indicated that all tube length cross-sections were approximately 50 mm × 50 mm in mid-sidewall outer dimension; however, the cross-section scans showed that there were localized sidewall profile and corner radii differences for tube specimens from different ID# lengths.

The overall results of the cross-section tracings and scans and the thickness measurements indicate that tube specimen geometry is "constant" within a single ID# tube length. Although a wall thickness adjustment may be necessary for the A36 tube specimen test results, geometric differences between specimens of different ID# lengths are not significant and configuration response differences may be attributed to material performance.

2.1.4. Material properties

To obtain indicators of strength levels and ductility and for quality control purposes, uniaxial tension testing was performed on the steel materials. For tube specimens ID#-3 for all tube lengths, sheet tensile specimens (ASTM E8-04) from the middle area of side 3 (sidewall opposite the weld) were waterjet machined on an Omax 55100 JetMachining Center (Engineer Research and Development Center (ERDC) – US Army Corps of Engineers) using 280-MPa water pressure and garnet grit. Additional water was sprayed onto the tube to minimize any heat generated during the cutting operation. The longitudinal axis of each tensile specimen was parallel with the longitudinal axis of the tube specimen. Uniaxial tension tests at 20 °C (room temperature) were performed using an MTS Universal Testing Machine (500 kN load frame and load cell – ERDC), a 50 mm gage length extensometer and a MTS computer-based data acquisition system. Testing was performed in the displacement control mode with the machine ram (top platen) speed set at approximately 2.5 mm/min. Data included time, load, and extensometer extension that was converted to engineering strain. The load was converted to engineering stress, and the engineering stress-engineering strain curves (subsequently referred to as the stress–strain curves) are shown in Fig. 5. The curves are plotted either to the 90% ultimate strength value after ultimate strength has been reached or to the limit of the extensometer, i.e. a strain of 0.50 mm/mm. The engineering yield stress and ultimate strength values are also given in Fig. 5. Data point pairs to generate approximations of the stress–strain curves for each material type are provided in Appendix A.

The ASTM A36 C2 and C4 materials have the lowest yield stress and tensile strength values of all of the materials in the study, but have very good ductility. The C2 and C4 tube length uniaxial tension test specimens have almost identical stress–strain curves and strength levels. From these results and the suppliers' information that a single length had been cut for shipment purposes, the tube specimens from the C2 and C4 lengths are considered to be the same material type and the single material type designation of A36-C2&C4 will be used for tube specimens from the C2 and C4 lengths.

The stress–strain curve for the ASTM A513 Type 1 material from the M1 tube length displayed behavior typical of low-carbon steel in an "annealed" condition, i.e., an initial elastic response, an upper yield point, a drop and fluctuation about an approximately constant stress value, also known as yield-point elongation, and then strain hardening behavior (Dieter, 1985). The A513-M1 material type has higher yield and ultimate strength values than the A36-C2&C4 material type; however, the A513-M1 material type has the lowest ductility of all the material types in the study. The 316SS-X1 material type has the highest yield stress of all the material types in the study. The material also displays significant strain hardening and ductility. For the AISI 304 stainless steel tubing, the stress–strain curve shapes are similar for materials from the S2, S3 and S4 tube lengths. Although the yield stresses for the 304SS-S2, -S3 and -S4 material types are lower than the yield stress of the 316SS-X1 material type, the 304SS stress–strain curves all cross over the 316SS curve and the 304SS material types have higher ultimate strengths than all of the other material types in the study. The 304SS material types also display exceptional ductility in that ultimate strengths occurred at engineering strains greater than the extensometer measuring capability and the stress–strain curves are therefore plotted only to a strain of 0.50 mm/mm.

For the AISI 304 stainless steel materials, when a small, hand-held magnet was moved over the surfaces of S2, S3 and S4 tube specimens in the "as-received" condition and across the transition and grip sections of

the tested S2, S3 and S4 uniaxial tension test specimens, no response to the magnet was felt. However, a positive attraction of the specimens to the magnet occurred when the magnet was moved over the uniform elongation and necked sections of the tested uniaxial tension specimens. This indicated that α'-martensite had formed and that the 304SS-S2, -S3 and -S4 material types have the ability to undergo the martensitic transformation.

As shown in Fig. 5, the strengths of all side 3 test specimens meet the minimum standard tensile requirements for their corresponding steel alloy and commercial grade. Because the geometry/fabrication-1 forming process involves cold-forming and welding, there is expected variation in material properties around the cross-sections and some strain-hardening of mid-sidewall material for a given tube length, but it is assumed that this cross-sectional variation is consistent or "constant" along the length. The order of the six material types based on increasing uniaxial tensile yield stress is A36-C2&C4, A513-M1, 304SS-S2, -S3 and -S4 and 316SS-X1, but based on increasing uniaxial tensile ultimate strength, the order changes to A36-C2&C4, A513-M1, 316SS-X1, and 304SS-S2, -S3 and -S4.

2.1.5. Design criteria for axial crush

Design criteria established to eliminate elastic global buckling and paneling response modes for square box components of mild- and high-strength steel were checked for each of the material types in the study. To prevent elastic column instability, the length criterion from the Euler buckling formula as given in strength of materials or elastic stability textbooks (for example, Bleich, 1952) requires that $L \leqslant L' = [\pi r_g (E/\sigma_y)^{1/2}/K_e]$ where L is the length of the undeformed test specimen column; L' is the upper limit on column length to prevent buckling; r_g is the radius of gyration of the column (same units as L); E is the modulus of elasticity; σ_y is the yield stress of the material (same units as E); and K_e is the effective length factor. Assuming a simply supported column ($K_e = 1$), the tube specimen length of 30.5 cm is less than the minimum calculated length, L', of 128 cm and elastic buckling will not occur for the specimens for any of the material types.

To prevent the paneling collapse of square box columns of mild- and high-strength steels, the compactness criterion (Mahmood and Paluszny, 1981) assumes a plate-type column under uniform axial compression and requires that the critical elastic local buckling stress be greater than the maximum (crippling) load-carrying strength of the component. In terms of a thickness and cross-sectional width ratio, t/b is required to be greater than or equal to $\{0.48[\sigma_y(1-\nu^2)/E]^{1/2}\}$, where t is the wall thickness; b is the width of the "buckling" plate (same units as t); σ_y is the yield strength of the material; ν is Poisson's ratio; and E is the modulus of elasticity (same units as σ_y). The minimum calculated t/b ratio of 0.028 for the steel material types is greater than the maximum required value of 0.023. Therefore, when axially loaded in compression, tube specimens from all of the geometry/fabrication-1 type tube lengths and without collapse initiators to reduce the peak load will not globally or locally buckle.

Overall results of the geometry measurements and material property testing indicate that tube specimens from the geometry/fabrication 1 type tube lengths have essentially the same overall geometry with the exception of the A36 tube specimens, which have slightly thinner wall thickness. Secondly, the material types included in the study allow for a variety of strength levels, strain hardening characteristics, and ductility values and for one material alloy, three strength levels are represented. Finally, tube specimens for all steel material types theoretically have the ability to undergo axial crush response.

2.2. Axial crush configuration response, experimental control techniques, and test setup

2.2.1. Symmetric axial crush mode Configuration A response

In prior research studies (DiPaolo, 2000; DiPaolo et al., 2004), the Configuration A response of the symmetric axial crush mode was established experimentally for 304SS welded, square box components. This was accomplished using control techniques consisting of end caps to constrain the tube specimen ends and collapse initiators in tube specimen sidewalls. The test specimens used in these studies were from the 304SS S1, S2, S3, and S4 tube lengths. The fold formation appearance and the load–displacement curve shape for the Configuration A response are shown in Fig. 2 for a prototype collapse initiator study test specimen, S1-18, and in Fig. 1 for the test specimen S1-7. The test specimen in Fig. 1 is in the "as-tested" orientation, and the specimen

shown in Fig. 2 is in an inverted orientation. Both orientations are used to compare fold formation aspects of axial crush specimens in the current study.

2.2.2. Experimental control techniques

2.2.2.1. End constraint – end caps. For a test specimen under axial compression, end conditions influence the local end deformation response; therefore, some form of end constraint is required to obtain consistent boundary conditions on all test specimens. For axial crush, end constraints affect the fold formation process in the initial phase that subsequently provides the initial deformation required for the secondary folding phase. In past research, tube end constraint has been achieved using end plates attached by welding or spot-welding to the specimens (Yamaya and Tani, 1971; Ohkubo et al., 1974; Chou, 1983; Lampinen and Jeryan, 1983; Yamaguchi et al., 1985; Wong et al., 1997) or grooved plates (Toda et al., 1976; DiPaolo, 1992). The welded plates require additional specimen preparation time and cost, and the welding process can cause distortions in the specimens and localized microstructural changes in the material. Grooved plates in the form of end caps have the advantage that they are removable and, therefore, reusable. However, the ability to reuse the caps for components with the same nominal cross-sectional dimensions requires that the width of the grooves allows for manufacturing tolerances on the tube specimens' cross-sections. Because the grooves will always be slightly wider than a specimen's outside width and slightly narrower than the specimen's inside width, the grooved end cap method cannot provide full fixity on the specimen ends. However, the end cap grooves do provide local support to specimen sidewall ends and their use can result in consistent end conditions from specimen to specimen.

The removable, grooved end caps that were used in the current investigation were designed, fabricated, and used in the prior research studies on 304SS welded, square box components (DiPaolo, 2000). Consistent end conditions were obtained for all specimens in that study. The caps are shown on a specimen during testing in Fig. 6a and, in detail, in Fig. 6b. Each cap was machined from a 100-mm-diameter, 25-mm-thick circular piece of AISI 4140 (Cr-Mo alloy) steel. After machining, caps were heat-treated and ground flat.

2.2.2.2. Collapse initiators – machined sidewall grooves. In past investigations of ductile metallic alloys, it has been shown that collapse initiators, also called triggers, stress concentrators, or imperfections, can be used

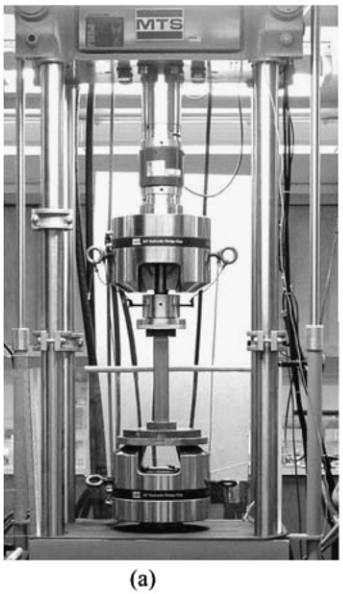

(a)

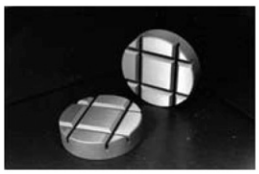

(b)

QUASI-STATIC TESTING

MTS universal testing machine
500 kN capacity
cross-head speed = 2.5 mm/min
displacement control
temperature - 20°C

(c)

Material designation	Specimen number	Axial crush test sequence number
Structural A36	C2-5	6
	C4-4	4
Mechanical A513 Tyl	M1-4	3
	M1-15	5
Stainless 316SS	X1-7	14
	X1-11	12
	X1-17	13
Stainless 304SS	S2-4	1
	S2-5-2	8
	S3-4	2
	S3-15-1	7
	S4-4	10
	S4-9	11
	S4-11	9

(d)

Fig. 6. Experimental axial crush testing: (a) MTS test machine and testing set-up, (b) grooved end cap set for tube end constraints, (c) testing conditions and (d) test specimens and sequence numbers.

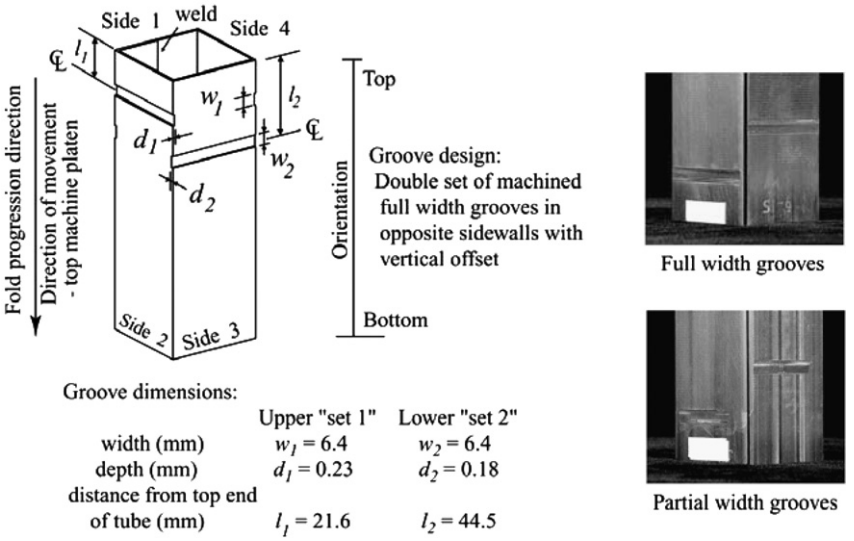

Fig. 7. Collapse initiator machined groove design and implementation.

to initiate a specific axial collapse mode; stabilize the collapse process; and for axial crush response, reduce the peak load magnitude or optimize another specific crush characteristic (Coppa, 1968; Thornton and Magee, 1977). The use of initiators also sets the start of the collapse process at a specific location on the specimen.

Collapse initiators consist of material and/or geometric modifications to the component. Examples of material modification initiators are locally annealed regions generated by concentrated heating, and the heat-affected zone generated by a weld. Types of geometric initiators include naturally formed and mechanically induced modifications (Thornton and Magee, 1977; Tani and Funahashi, 1978; Chou, 1983; Lampinen and Jeryan, 1983; Gupta and Gupta, 1993; Abah et al., 1998; Marshall and Nurick, 1998) and have the advantages of being visually detectable and controllable by dimension adjustment.

Collapse initiators were used in the investigation to set the axial locations for the initial inward collapse of all four sidewalls for a tube specimen, to control the fold formation in the initial phase of the crush, and to establish the specific deformation conditions required for the natural secondary fold formation phase of a specific axial crush configuration response. The collapse initiator design consisted of a double set of transverse, full sidewall width, machined grooves in opposite sidewalls with a vertical offset for groove pairs in adjacent sidewalls. An undeformed tube specimen with grooves is shown in Fig. 1. The design was developed in preliminary collapse initiator testing (DiPaolo, 2000) of prototype specimens from the 304SS S1 through S4 tube lengths. The location and spacing of the grooves was based on the geometry of the natural wavelength in the initial fold formation phase of the 304SS specimens that had been tested with end caps but without initiators and that had undergone configuration responses similar to the Configuration A response shown in Fig. 2.

For the design of the 304SS collapse initiators, the width of the grooves was set at slightly less than the curve length of the corresponding inward fold on an unmodified specimen for the configuration response, and the groove depth of 10–15% of the wall thickness was used to induce localized bending moments in the sidewalls without disrupting the fold formation process. Throughout the current study on the steel materials, the same groove design was used for tube specimens of all material types. No adjustment in the dimensions was made to account for wall thickness or material strength differences. The geometry and dimensions for the groove design are given in Fig. 7.

The grooves were machined at the "end of cutting" end for all tube specimens and were produced using an end mill cutter in a milling machine. In previous research, multiple passes were made to ensure a full width groove on each sidewall. In the current research, only one pass was made for each groove. Because some sidewalls had slight outward curvatures, full-sidewall width grooves were not obtained on all walls for all material

types. Examples of full width and partial width grooves are shown in Fig. 7. No blending of the grooves to the original tube outside surface was done.

2.2.3. Test setup and procedure

In the current study, geometry, material, and square tube-forming fabrication processing, test specimen end constraints, collapse initiator design, and testing conditions were held constant. The general procedure for the study consisted of selecting a specific displacement point on the load–displacement curve of a prototype test specimen for the Configuration A response and, if the configuration response was being obtained for a specimen, the axial crush of the specimen was continued to that specific point. Because the end caps do not provide total fixity to the tube specimen ends, some variation in the load–displacement curve shape in the initial phase of the axial crush response was to be expected from specimen to specimen. Therefore, the specific displacement point on the Configuration A load–displacement curve shape was chosen to be the end point of the second cycle of the secondary folding phase. This would provide data on two full cycles in the secondary folding phase to verify that the specimens underwent the axial crush Configuration A response.

For each material type, two or three tube specimens were selected for axial crush testing. A total of 14 tube specimens were chosen and the specimen numbers are given in Fig. 6d. For each tube specimen, square grid patterns based on an orthogonal line set were processed onto the exterior of all four sidewalls using photoresist processes, and all exterior cornerlines were marked using a Sanford Sharpie® permanent marker. Masking tape shims were placed on the sidewall centers on both ends of each tube specimen in a symmetric manner (equal number of layers for opposite sidewalls) to obtain a "tight" fit and ensure centering of the specimen in the end cap grooves. Shims were placed on the inside for sidewalls 1 and 3 and on the outside for sidewalls 2 and 4.

All axial crush testing was quasi-static at 20 °C using an MTS universal testing machine (500 kN load frame and load cell – ERDC). The testing mode was displacement control with the top platen of the machine being moved vertically downward to compress the tube specimens. The ram speed was 2.5 mm/min. The test set-up and conditions are shown in Fig. 6a and c, respectively. The test sequence numbers for the test specimens are given in Fig. 6d. For each test, a specimen with end caps was placed vertically in the testing machine with the specimen's collapse initiator grooves near the top platen. Therefore, the folding direction in the specimen was downward and in the same direction as the upper platen's movement. Computer data included time, load, and crosshead displacement at a recording rate of one data point every 2 s. Load–displacement curves were generated directly from the computer data.

For each test specimen, axial crush Configuration A response would be verified using both fold appearance and load–displacement curve shape. For the specimens that had undergone the Configuration A response, crush characteristic data in the initial phase and for cycles in the secondary phase were tabulated and compared within a material type and among material types.

3. Experimental investigation results

3.1. Fold formation process, load–displacement curves and crush characteristics

For all of the 14 specimens tested, collapse initiated at the machined grooves; fold formation progressed down the longitudinal axis of the specimens; and the mode of response was the symmetric axial crush mode. The final permanent fold formation of Corner 34 for all of the specimens of a material type is shown in a photograph in Fig. 8 for each of the six material types. Beside the photograph, the load–displacement curves for all of the specimens of the corresponding material type are superimposed. For a given material type, differences in the load–displacement curves occurred mainly in the initial phase, as anticipated, and for the 304SS-S3 specimens, a small offset of the curves occurred at the beginning of the secondary phase for the two test specimens. In general, the fold formation is consistent from specimen to specimen, and excellent point-to-point repeatability of the load–displacement curve was obtained for specimens within each material type.

One specimen from each material type was chosen, and Fig. 9a shows the side 3-fold formation for these specimens. Using the same color for a material type as was used for the uniaxial tensile test stress–strain curves in Fig. 5 and the load–displacement curves in Fig. 8 (see Fig. 9b for the color key), the complete

load–displacement curves for all 14 test specimens are superimposed in Fig. 9c. The load–displacement curve shapes in the secondary folding phase were evaluated by separating the curves into cycle sections at the minimum loads. The sections were then horizontally shifted and aligned with respect to the maximum load points in the cycle section. For all 14 test specimens, the shifted and aligned load–displacement cycle section curves are superimposed in Fig. 9d and show that the variation in load–displacement curves is minimal for specimens within a material type. Visual comparisons of fold formations and curve shapes with those of the prototype specimen S1-18 (see Fig. 2) indicated that all specimens for all material types underwent the Configuration A response.

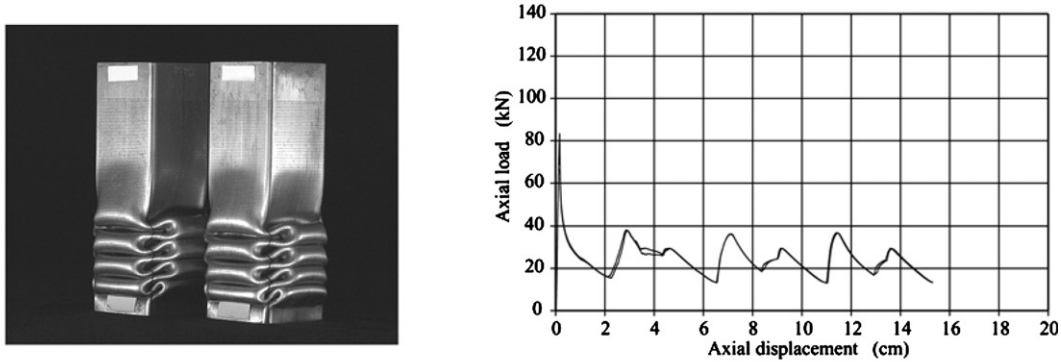

A36 steel - C2-5 and C4-4

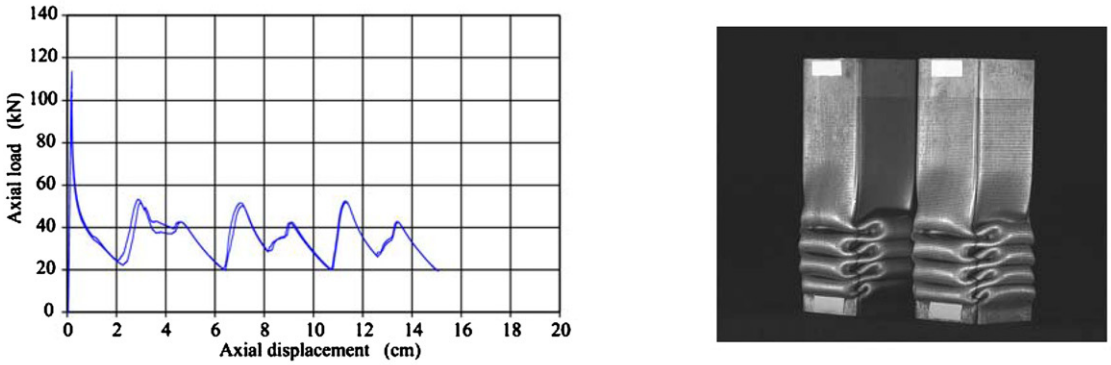

A513 steel - M1-4 and M1-15

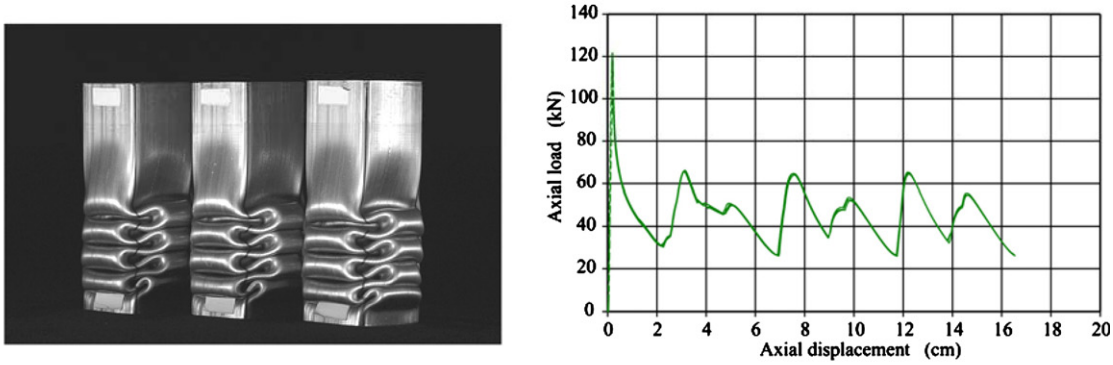

316 stainless steel - X1-7, X1-11 and X1-17

Fig. 8. Fold formation and axial load–displacement curves – individual material types.

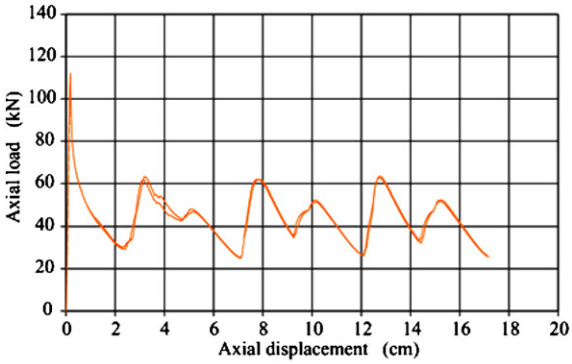

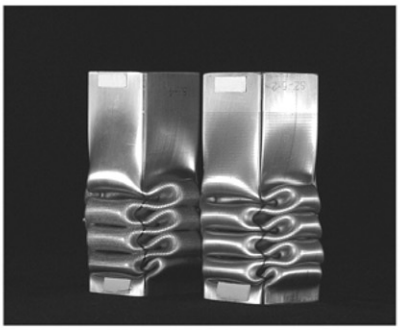

304 stainless steel - S2-5-2 and S2-4

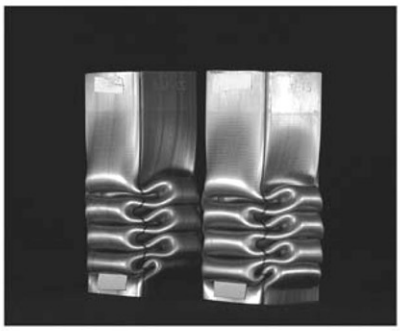

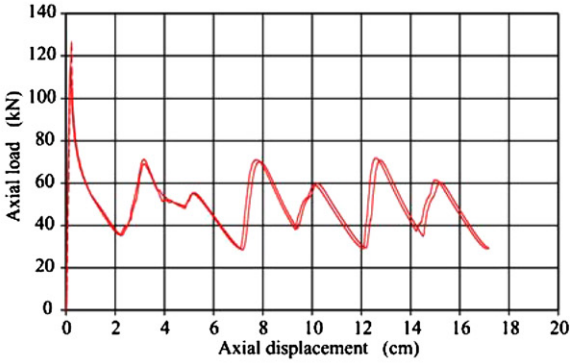

304 stainless steel - S3-4 and S3-15-1

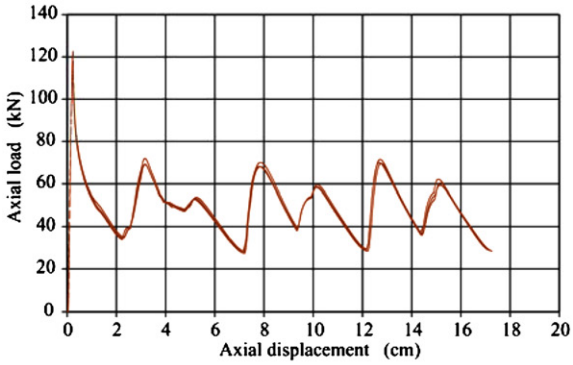

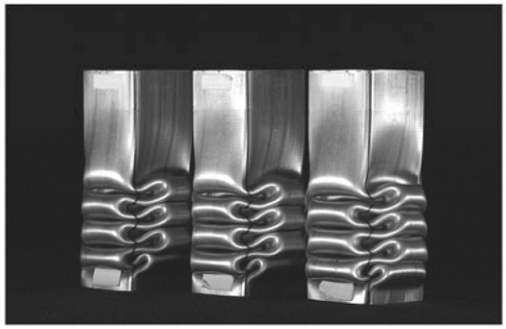

304 stainless steel - S4-4, S4-9 and S4-11

Fig. 8 (*continued*)

To evaluate the Configuration A response for each material type, crush characteristics were analyzed for the initial phase and both cycle 1 and cycle 2 of the secondary folding phase (see Fig. 1c). The analysis was performed calculating percent differences using an average value basis. For each material type, values for a specific crush characteristic were summed for all specimens of that material type and then an average value was calculated by dividing the sum by the number of specimens. A percent difference corresponding to each value was calculated by subtracting the value from the average, dividing the difference by the average, converting the fraction to a percentage (multiplying by 100) and taking the absolute value. Finally, for each material type, the

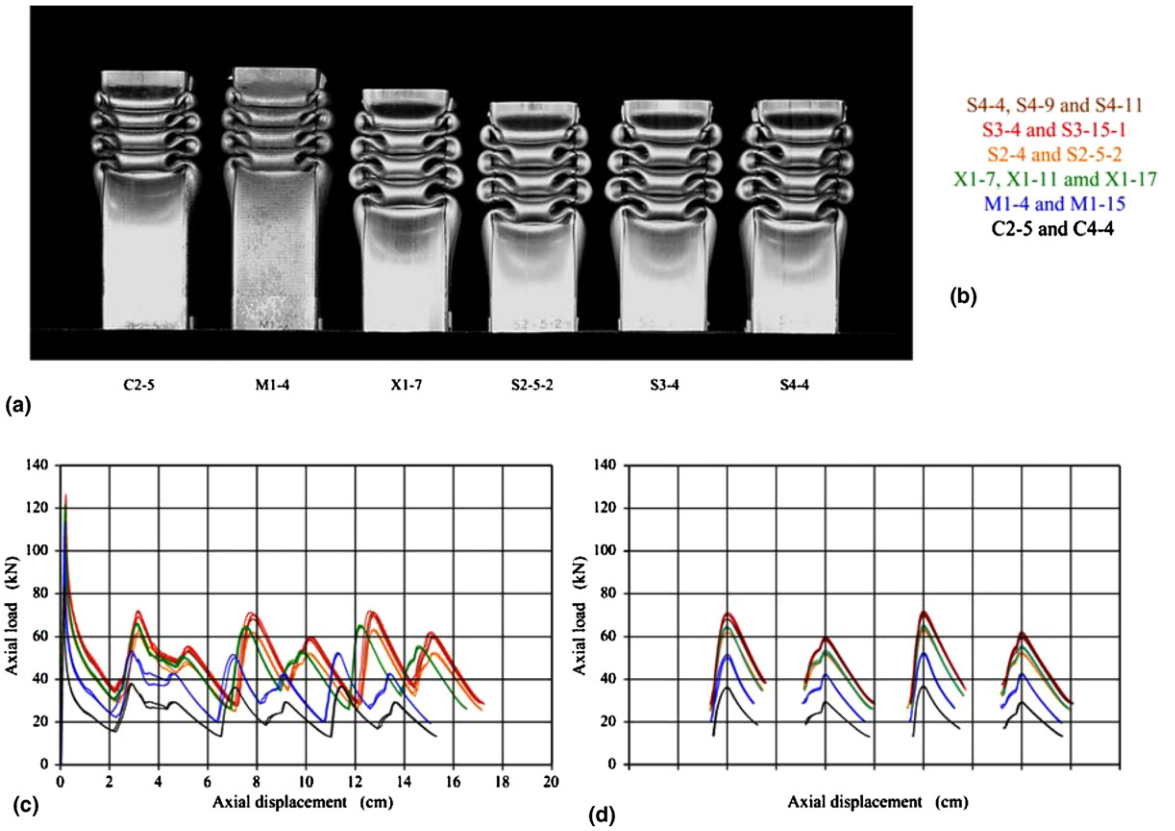

Fig. 9. Fold formation and superimposed load–displacement curves: (a) example quasi-static axial crush specimens, (b) color key for curves, (c) superimposed load–displacement curves (all 14 quasi-static axial crush specimens) and (d) superimposed secondary folding phase curve sections (all 14 quasi-static axial crush specimens).

Table 1
Crush characteristics – initial folding phase

Steel	ASTM or AISI no.	Specimen	Load (kN)					Maximum % diff.	EA_0 (kN cm)	δ_0 (cm)	$P_{\text{mean}\theta}$ (kN)	Maximum % diff.
			$P_{\max}$ (P_{02})	(P_{03})	(P_{04})	(P_{05})	(P_{06})					
Structural	A36	C2-5	77.9	15.4	37.8	26.6	29.4		167	6.53	25.5	
		C4-4	83.3	15.9	38.1	26.5	26.9	4.5	168	6.54	25.7	0.5
Mechanical	A513 Ty 1	M1-4	106.8	22.2	51.6	39.4	42.6		232	6.36	36.5	
		M1-15	113.4	24.2	53.2	37.1	42.5	6.4	238	6.43	37.0	1.2
Stainless	316	X1-7	118.1	30.6	65.7	45.8	50.3		320	6.92	46.2	
		X1-11	121.4	30.2	66.1	45.5	49.8		321	6.95	46.2	
		X1-17	121.6	30.6	65.6	46.2	50.8	1.9	320	6.87	46.6	1.0
Stainless	304	S2-4	112.2	29.2	63.2	43.1	48.2		318	7.13	44.6	
		S2-5-2	105.8	30.1	61.7	42.6	46.9	2.9	313	7.10	44.0	
		S3-4	114.9	35.3	69.1	48.1	55.0		361	7.10	50.9	
		S3-15-1	126.5	35.3	71.2	49.0	55.4	4.8	367	7.19	51.0	0.8
		S4-4	117.9	34.8	71.9	48.2	53.7		362	7.15	50.6	
		S4-9	122.6	34.3	69.1	47.5	52.8		353	7.17	49.3	
		S4-11	111.7	33.9	69.0	47.1	53.1	4.8	355	7.21	49.2	1.8

Table 2
Crush characteristics – secondary folding phase – maximum and minimum load magnitudes

Steel	ASTM or AISI no.	Specimen	Load (kN)									Maximum % diff.
			P_{11}	P_{12}	P_{13}	P_{14}	P_{21} (P_{15})	P_{22}	P_{23}	P_{24}	P_{31}(P_{25})	
Structural	A36	C2-5	13.4	36.0	18.6	29.5	13.1	36.8	16.8	29.4	13.3	
		C4-4	13.2	36.3	18.5	29.4	13.0	36.6	16.8	29.2	13.3	0.9
Mechanical	A513 Ty 1	Ml–4	20.3	51.6	28.4	42.2	20.0	52.4	26.8	42.7	19.9	
		M1-15	19.7	50.1	28.7	42.5	19.9	51.7	26.1	42.3	19.3	1.7
Stainless	316	X1-7	26.2	64.7	35.0	53.6	26.4	65.3	33.0	55.6	26.8	
		X1-11	26.0	63.9	34.7	52.0	25.9	64.3	32.1	54.6	26.1	
		X1-17	26.3	64.4	34.5	52.6	26.1	64.7	33.2	54.8	26.2	2.1
Stainless	304	S2-4	25.2	62.0	35.5	51.5	26.4	62.7	33.0	51.9	25.4	
		S2-5-2	24.9	62.0	34.6	52.4	26.0	63.4	32.0	52.5	26.2	1.6
		S3-4	28.8	71.1	38.0	59.1	29.1	71.8	37.3	61.5	28.9	
		S3-15-1	28.3	70.1	38.4	59.9	29.3	70.8	34.9	60.3	29.1	3.4
		S4-4	28.4	70.0	39.4	59.5	29.4	71.4	37.3	59.3	28.7	
		S4-9	27.4	68.2	38.0	58.3	28.5	70.0	36.0	62.1	28.8	
		S4-11	27.4	68.0	39.0	58.6	28.3	69.6	35.9	60.4	28.4	2.5

Table 3
Crush characteristics – secondary folding phase – energy absorption, cycle displacement and mean load magnitudes

Steel	ASTM or AISI no.	Specimen	Energy absorption (kN cm)		Cycle displacement (cm)		Mean load (kN)		Maximum % diff.
			EA_1	EA_2	δ_1	δ_2	P_{mean1}	P_{mean2}	
Structural	A36	C2-5	106	102	4.44	4.33	23.9	23.6	
		C4-4	106	101	4.48	4.28	23.7	23.5	0.7
Mechanical	A513 Ty 1	Ml–4	152	149	4.35	4.34	35.0	34.4	
		M1-15	149	147	4.32	4.32	34.5	33.9	1.0
Stainless	316	X1-7	218	217	4.79	4.78	45.5	45.4	
		Xl-11	215	214	4.80	4.80	44.8	44.6	
		Xl-17	217	217	4.82	4.85	45.0	44.7	1.1
Stainless	304	S2-4	220	222	4.93	5.13	44.5	43.3	
		S2-5-2	221	220	5.00	5.03	44.2	43.8	1.1
		S3-4	249	250	4.99	5.03	50.0	49.7	
		S3-15-1	249	245	5.01	5.00	49.7	49.1	0.9
		S4-4	251	245	5.01	5.00	50.0	49.1	
		S4-9	244	249	4.99	5.04	49.0	49.3	
		S4-11	245	246	5.00	5.06	48.9	48.7	1.7

maximum of all of the percent differences for all of the load crush characteristics and the maximum of the percent differences for the energy absorption, displacement, and mean load crush characteristics were determined for each phase. Table 1 provides the initial phase analysis results. For all material types, maximum percent differences were less than or equal to 7% for load magnitudes and 2% for energy absorption, displacement, and mean load quantities. For the secondary folding phase, minimum and maximum load magnitude data are given in Table 2, and energy absorption, displacement, and mean load data are given for cycle 1 and cycle 2 in Table 3.

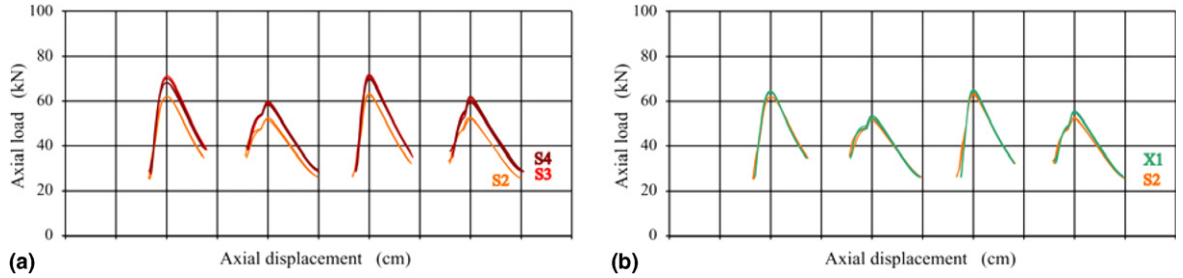

Fig. 10. Comparisons of secondary folding phase curve sections for 304SS and 316SS materials: (a) superimposed curve sections for 304SS-S2, -S3 and -S4 specimens (seven specimens) and (b) superimposed curve sections for 304SS-S2, and 316SS-X1 specimens (five specimens).

For all material types, maximum percent differences were less than or equal to 4% for load magnitudes and 2% for energy absorption, displacement, and mean load. The higher percent differences for the load magnitudes in the initial phase compared to the secondary phase may be attributed to the incomplete fixity of tube specimen ends in the end caps.

For the A36-C2&C4, A513-M1 and the 304SS material types, the superimposed load–displacement cycle section curves in Fig. 9d display an upward shift on a point-to-point basis consistent with increase in material strength as represented by the mid-sidewall 3 uniaxial tension test results. For the 304SS material types, superimposed load–displacement curves are shown again in Fig. 10a. It can be seen that the curves for the 304SS-S2 material type specimens are significantly lower than the curves for the higher strength 304SS-S3 and -S4 material type specimens and there is little difference in the Configuration A response between the 304SS-S3 and 304SS-S4 material type specimens. This trend is also consistent with the uniaxial tension test results for the 304SS material types.

However, the photo and superimposed curves in Fig. 9 also indicate differences in Configuration A response for the material types. The fold formation photo in Fig. 9a shows that the traveling foldlines of the lower strength A36-C2&C4 and A513-M1 specimens remain closer to the cornerlines and, as shown in Fig. 9d, the specimens of these material types have smaller cycle section displacements than the higher strength stainless steels. Also, although the A513-M1 material type has higher tensile strength than the A36-C2&C4 material type and the A513-M1 load–displacement curves have higher load magnitudes on a point-to-point basis than the A36-C2&C4 curves, the A513-M1 axial crush specimen cycle displacements are slightly less than those of the A36-C2&C4 axial crush specimens. Finally, as shown in Figs. 9 and 10b, there is little difference in cycle section curves for the 304SS-S2 and 316SS-X1 specimens, but the 316SS-X1 stress–strain curve is above the highest strength 304SS material type curve for low strains around the yielding region and curves over until it is below the lowest strength 304SS curve after ultimate strength has been reached (see Fig. 5).

Finally, a small hand-held magnet was placed close to and moved over the outside surfaces of the 316SS-X1 and the 304SS-S2, -S3 and -S4 axial crush test specimens. For the 316SS-X1 specimens, no response to the magnet was apparent at any location. For specimens of all three 304SS material types, no response was apparent on the mid-sidewall fold areas; however, a positive response indicated that the martensitic transformation had occurred at corner locations and along the traveling foldlines.

Future research including deformation and microstructure studies is required to investigate in more detail the differences observed in axial crush configuration response for the material types. The research could include study of the transformation of austenite to α'-martensite and ε-martensite during the fold formation process for the AISI 304 SS materials to further the understanding of localized material performance during the axial crush fold formation process.

3.2. Comparison of results with previous studies

For the 304SS-S2 and -S3 material types, tube specimens S2-10-3 and S3-18 had been tested in a past axial crush research study that established control methods to obtain Configuration A response (DiPaolo, 2000).

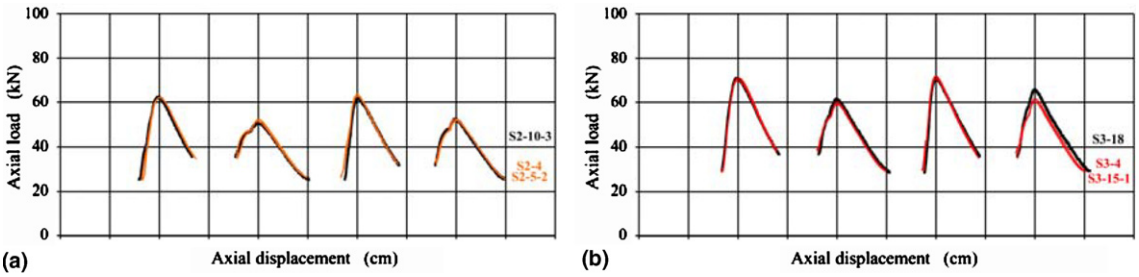

Fig. 11. Comparisons of secondary folding phase curve sections for 304 stainless steel materials – current and past research: (a) superimposed curve sections for S2-4, S2-5-2 and S2-10-3 (three specimens) and (b) superimposed curve sections for S3-4, S3-15-1 and S3-18 specimens (three specimens).

Table 4
Crush characteristics – current vs. past research 304 stainless steel specimens secondary folding phase

Steel	ASTM or AISI no.	Specimen	Load (kN)									Maximum % diff.
			P_{11}	P_{12}	P_{13}	P_{14}	$P_{21}(P_{15})$	P_{22}	P_{23}	P_{24}	P_{31} (P_{25})	
Stainless	304	S2 ave	25.0	62.0	35.1	52.0	26.2	63.0	32.5	52.2	25.8	3.9
		S2-10-3	25.2	62.1	35.6	51.0	25.2	61.9	31.7	52.6	25.6	
		S3 ave	28.6	70.6	38.2	59.5	29.2	71.3	36.1	60.9	29.0	8.0
		S3-18	29.3	71.0	36.5	61.9	28.0	71.0	35.8	65.8	28.7	

	Energy absorption (kN cm)		Cycle displacement (cm)		Mean load (kN)		Maximum % diff.
	EA_1	EA_2	δ_1	δ_2	P_{mean1}	P_{mean2}	
S2 ave	220	221	4.96	5.08	44.4	43.6	3.0
S2-10-3	223	216	5.11	5.00	43.6	43.3	
S3 ave	251	249	5.00	5.01	50.2	49.7	4.9
S3-18	258	260	5.18	5.17	49.8	50.2	

Testing conditions were similar to those in the current study in that the end caps in Fig. 6 and the groove design in Fig. 7 were used; specimen sidewalls were shimmed as described above; and testing was quasi-static, displacement control mode at a ram speed of 2.5 mm/min and at 20 °C. However, grooves were machined using several passes of increasing depth to obtain full width grooves, and testing was performed using a 1350-kN-capacity MTS universal testing machine (MTS Load Frame 1000/2000 kN – University of California at Berkeley) for which the bottom platen of the machine moved vertically upward to load the tube specimens in compression. As each specimen with end caps was placed vertically in the testing machine with the specimen's collapse initiator grooves nearest the top platen, the folding direction in the specimen was downward and opposite to the bottom platen's upward movement.

The secondary folding phase cycle sections are superimposed for the current study specimens S2-4 and S2-5-2 and the past study specimen S2-10-3 in Fig. 11a and for the current study specimens S3-4 and S3-15-1 and the past study specimen S3-18 in Fig. 11b. Crush characteristics for specimens S2-10-3 and S3-18 are given in Table 4 and compared with the current study 304SS-S2 and 304SS-S3 material types average test values, respectively. Maximum percent differences for load magnitudes are less than 8% and for energy absorption, cycle displacement and mean load, maximum percent differences are less than 5%. The superimposed curves and crush characteristic analysis show excellent repeatability of results between the two studies.

3.3. Configuration A response mean crushing load prediction

Equations to predict axial crush characteristics of commercially produced tubing would be valuable tools in the preliminary design phase of axial crush energy absorbers. For square box components, mathematical models have been generated in past research investigations to relate quasi-static axial crush characteristics to geometric and material parameters and to predict performance (Wierzbicki and Abramowicz, 1983; Abramowicz and Jones, 1984; Magee and Thornton, 1979; Wierzbicki and Abramowicz, 1989). The resulting equations have been based on modeling the mechanics and kinematics of the folding process. In particular, several equations for the mean crushing load, P_m, have been developed for a square column assuming homogeneous, isotropic, rigid perfectly plastic material with equivalent time- and temperature-independent behavior in uniaxial tension and compression and no corner geometry effects. For a single value of, but otherwise arbitrary, flow stress, σ_0, where $\sigma_{ty} \leqslant \sigma_o \leqslant \sigma_{tu}$, and σ_{ty} and σ_{tu} are the true "yield" stress and true ultimate strength, respectively, and using $M_0 = \sigma_0 t^2/4$, where t is the wall thickness, the equations are of the form:

$$P_m/M_0 = C(b/t)^x \quad \text{or} \quad P_m = C' b^x t^{(2-x)}.$$

For the equation with values for the coefficients of $C = 52.22$ or $C' = 13.06$ and $x = 0.33$ (Abramowicz and Jones, 1984), formulae have been referenced that modify the flow stress to take into account strain hardening of the material during the fold formation process (Langseth and Hopperstad, 1996; Hanssen et al., 1999; White et al., 1999; Santosa et al., 2000).

Because the results of the current investigation provide symmetric axial crush mode data for specimens with different uniaxial tensile material strengths, strain hardening behavior and ductility levels, calculations were performed and comparisons between test and analytical mean crushing load values were made using the above equation with the $C' = 13.06$ and $x = 0.33$ coefficients. Two sets of calculations were performed with the understanding that several assumptions upon which the above equation is based are not valid for the tube specimens in this study. Because of the square tube forming process, the material around the cross-section is not homogeneous and there is a corner geometry effect due to the rounded corners. Uniaxial tensile properties from the mid-sidewall side 3 area may not be appropriate for use in calculating an equivalent flow stress for the fold formation process in the corner areas. Finally, the assumption of equal material response in tension and compression may not be valid for the 304SS material types because of the occurrence of the martensitic transformation in the foldline areas.

For the first set of calculations, the measured uniaxial tensile strengths were used and no attempt was made to adjust for prior strain hardening of material during fabrication, as the amount for each material type was unknown at the time. Minimum percent differences based on the test values were obtained using the measured engineering yield stress for the A36-C2&C4 and the A513-M1 material types and the average of the engineering yield stress and engineering ultimate strength for the 316SS-X1 and the 304SS-S2, -S3 and -S4 material types. The mean crushing loads were overestimated by less than 15% for all material types.

Another set of calculations was performed to address the fact that an engineer may only know the material alloy and have only standard specifications and their minimum required strength levels available at the time of design. Minimum percent differences based on the test values were obtained using the tensile requirements for round structural tubing Grade A (ASTM A500-03a) for the A36-C2&C4 material type and the 1/16 hard tensile property requirements (ASTM A666-03) for the 316SS-X1 and the 304SS-S2, -S3 and -S4 material types and the average of the true yield stress and true ultimate strength values. The mean crushing load was overestimated by less than 5% for the A36-C2&C4 material type and less than 10% for all of the stainless steel material types. For the A513-M1 material type, the minimum percent difference was obtained using the 1015 tensile properties for round tubing (ASTM A513-00) and the true ultimate strength values. The mean crushing load was overestimated by less than 2%. The use of the true ultimate strength values for the A513-M1 material type may be reasonable because the material type has "low" tensile ductility and the strain at the true ultimate strength of the A513-M1 material type is of a similar magnitude to the strain values for the average of the true yield stress and the true ultimate strength for the other material types.

Further research is required to validate or modify the current formula or to develop other predictive crush performance equations for the material types and the geometry/fabrication-1 cross-section used in this study

and the Configuration A response. This research would include investigating local material property variation around the tubing cross-section due to the square tube forming operations; studying other locations for the uniaxial tensile material property testing or other types of and locations for mechanical properties to relate to axial crush characteristics; and obtaining Configuration A response crush characteristic data for other square tube width and wall thickness geometries.

4. Conclusions and future research

An experimental investigation on symmetric axial crush response was performed on thin-walled, ductile steel, square box components. For quasi-static testing conditions using end caps for tube end constraints and transverse machined partial-to-full sidewall width grooves for collapse initiators, axial crush of ASTM A36 and A513 Type 1 plain low-carbon steel and AISI 304 and 316 austenitic stainless steel tube specimens in a single geometry/fabrication process was restricted to the same specific configuration response (fold formation and load–displacement curve shape). Within a material type, percent differences on an average value basis were less than or equal to 7% for minimum and maximum load magnitudes and 2% for energy absorption, displacement, and mean load for the initial phase and the first two cycles of the secondary folding phase. The results demonstrate the ability to restrict symmetric axial crush mode response to a specific configuration and ensure repeatable load magnitudes and an energy absorption process for commercially produced, steel box components of material types with significantly different uniaxial tensile strength levels, strain hardening behaviors and ductility values.

During the course of the investigation, it was also found that partial sidewall width grooves were adequate to initiate collapse and establish the required configuration response and that excellent repeatability of crush characteristics could be obtained independent of test machine and direction of loading with respect to the collapse initiator tube specimen end. However, for one of the two commercially produced square tubing geometry/fabrication process cross-sections that were obtained for the study, material failure occurred along two cornerlines as the fold formation process progressed along the longitudinal axis of the tube specimens. Further investigations are required to study cross-sectional material variation and material properties resulting from square tube fabrication processes and with respect to stress/strain states critical to the axial crush process. More research is also required to study Configuration A response of other square tube geometries. For engineering design estimation purposes, results of these investigations could be used to further the development of equivalent material strength measures for input into existing crush characteristic formulae or to establish specific formulae that represent a configuration response of a given fabricated product form. For engineering application research purposes, the results could be used to more fully understand severe plastic deformation and failure limits of materials for high-energy absorption responses.

Acknowledgements

The authors wish to extend our appreciation to the ERDC Directorate of Public Works machine shop and model shop personnel for their fine efforts in specimen preparation. We also gratefully acknowledge the support and encouragement of the research work by Dr. Robert L. Hall and Dr. Reed L. Mosher. Permission to publish was granted by Director, Geotechnical and Structures Laboratory, ERDC. Approved for public release – distribution is unlimited.

Appendix A

Table A1 provides points that can be used to generate approximations of the uniaxial tension engineering stress-engineering strain curves shown in Fig. 5. For a given material type, the number and spacing of strain magnitudes were selected to accommodate curve shape variations. For each strain magnitude, the stress was calculated using linear interpolation between stress–strain test data point pairs that bounded the corresponding strain magnitude. The modulus of elasticity used in the calculations was 207 MPa for the A36-C2&C4 and the A513-M1 material types and 193 MPa for the 316SS-X1 and the 304SS-S2, -S3 and -S4 material types. The strain magnitudes given in the table are total strain values.

Table A1
Engineering strain and engineering stress point pairs

A36-C2&C4		A513-M1		316SS-X1		304SS	-S2	-S3	-S4
ε_{engr} (mm/mm)	σ_{engr} (MPa)	ε_{engr} (mm/mm)	σ_{engr} (MPa)	ε_{engr} (mm/mm)	σ_{engr} (MPa)	ε_{engr} (mm/mm)	σ_{engr} (MPa)	σ_{engr} (MPa)	σ_{engr} (MPa)
0.0020	311.6	0.0020	343.7	0.0035	441.5	0.0035	369.6	398.2	415.2
0.0030	333.3	0.0025	379.0	0.0040	459.8	0.0040	380.1		
0.0036	336.8	0.0030	399.9	0.0044	468.0	0.0042		419.7	
0.0040	338.3	0.0035	396.1	0.0050	483.5	0.0043			439.3
0.0050	340.0	0.0050	396.9	0.0075	507.6	0.0050	396.8	437.4	454.6
0.0075	343.0	0.0075	397.1	0.010	516.6	0.0075	414.0	461.3	477.4
0.010	345.6	0.010	396.8	0.020	533.2	0.010	421.4	473.1	488.3
0.020	352.6	0.014	400.7	0.030	544.0	0.020	438.0	492.1	507.1
0.030	355.8	0.020	414.1	0.040	554.5	0.030	451.6	506.0	521.5
0.040	357.4	0.030	427.5	0.050	564.7	0.040	463.6	519.7	535.6
0.050	358.5	0.040	437.3	0.075	588.4	0.050	475.5	532.9	548.9
0.100	362.4	0.050	442.4	0.100	606.7	0.100	528.9	591.8	607.7
0.175	365.1	0.060	445.3	0.125	623.5	0.150	569.6	635.5	652.3
0.200	363.9	0.070	446.0	0.150	636.3	0.200	602.1	668.2	684.0
0.250	362.4	0.080	446.5	0.200	655.5	0.250	625.3	690.5	708.8
0.270	361.7	0.090	446.2	0.250	666.9	0.300	643.9	707.0	725.2
0.290	359.7	0.095	447.5	0.300	675.2	0.350	657.9	720.1	737.9
0.300	358.3	0.100	445.5	0.357	679.0	0.400	667.8	728.5	747.5
0.310	356.8	0.120	443.3	0.400	677.3	0.450	675.5	735.1	754.0
0.330	350.0	0.135	440.9	0.420	674.2	0.500	680.6	738.6	758.6
0.350	336.4	0.150	432.1	0.430	670.3				
0.356	329.5	0.155	426.9	0.440	664.0				
		0.160	420.7	0.450	653.1				
		0.168	403.0	0.460	620.8				
				0.462	604.0				

References

Abah, L., Limam, A., Dejeammes, M., 1998. Effects of cutouts on static and dynamic behaviour of square aluminium extrusions. In: Jones, N., Talaslidis, D.G., Brebbia, C.A., Manolis, G.D. (Eds.), Structures Under Shock and Impact V – SUSI 98. Computational Mechanics Publications, Southampton, UK, pp. 133–142.

Abramowicz, W., Jones, N., 1984. Dynamic axial crushing of square tubes. International Journal of Impact Engineering 2 (2), 179–208.

Abramowicz, W., Wierzbicki, T., 1979. A kinematic approach to crushing of shell structures. In: Record of Conference Papers – Annual Petroleum and Chemical Industry Conference – International Conference on Vehicle Structural Mechanics, 3rd, October 10–12, 1979, Troy, MI, P-83 (790992). Society of Automotive Engineers, Warrendale, PA, pp. 211–223.

Andrews, K.R.F., England, G.L., Ghani, E., 1983. Classification of the axial collapse of cylindrical tubes under quasi-static loading. International Journal of Mechanical Sciences 25 (9–10), 687–696.

Angel, T., 1954. Formation of martensite in austenitic stainless steels – effects of deformation, temperature, and composition. Journal of the Iron and Steel Institute (May), 402–412.

ASTM Designation: A 36/A 36M-05, 2005. Standard specification for carbon structural steel. Annual Book of ASTM Standards 2005, Section 1, Iron and Steel Products, Volume 01.04, Steel – Structural, Reinforcing, Pressure Vessel, Railway. American Society for Testing and Materials (ASTM), West Conshohocken, PA.

ASTM Designation: A 500-3a, 2005. Standard specification for cold-formed welded and seamless carbon steel structural tubing in rounds and shapes. Annual Book of ASTM Standards 2005, Section 1, Iron and Steel Products, Volume 01.01, Steel – Piping, Tubing, Fittings. ASTM, West Conshohocken, PA.

ASTM Designation: A 513-00, 2005. Standard specification for electric-resistance-welded carbon and alloy steel mechanical tubing. Annual Book of ASTM Standards 2005, Section 1, Iron and Steel Products, Volume 01.01, Steel – Piping, Tubing, Fittings. ASTM, West Conshohocken, PA.

ASTM Designation: A 666-03, 2005. Standard specification for annealed or cold-worked austenitic stainless steel sheet, strip, plate, and flat bar. Annual Book of ASTM Standards 2005, Section 1, Iron and Steel Products, Volume 01.03, Steel – Plate, Sheet, Strip, Wire; Stainless Steel Bar. ASTM, West Conshohocken, PA.

ASTM Designation: E 8-04, 2005. Standard test methods for tension testing of metallic materials. Annual Book of ASTM Standards 2005, Section 3, Metals Test Methods and Analytical Procedures, Volume 03.01, Metals – Mechanical Testing; Elevated and Low-Temperature Tests; Metallography. ASTM, West Conshohocken, PA.

Bleich, F., 1952. Buckling Strength of Metal Structures. McGraw-Hill Book Company, Inc., New York.

Buehler, 2003. 2003 Consumables Buyer's Guide. Buehler Ltd., Lake Bluff, IL, USA.

Chou, C.C., 1983. The measurement of impact forces under dynamic crush using a drop tower test facility. In: International Congress and Exposition, February 28–March 4, 1983, Detroit, MI (830467). Society of Automotive Engineers, Warrendale, PA, pp. 1–16.

Coppa, A.P., 1968. New ways to soften shock. Machine Design (March 28), 130–140.

Dieter, G.E., 1985. Mechanical behaivior of materials under tension. In: Davis, J.R., Refsnes, S.K. (Eds.), Mechanical Testing, Metals Handbook, vol. 8, ninth ed.. American Society for Metals, Metals Park, OH, pp. 20–27.

DiPaolo, B.P., 1992. An experimental and analytical investigation of the axial crush of an aluminum box section. Unpublished MS Thesis, Department of Civil Engineering, School of Engineering, University of Pittsburgh, Pittsburgh, PA.

DiPaolo, B.P., 2000. An experimental investigation on the axial crush of a thin-walled, stainless steel box component. Ph.D. Dissertation, Department of Civil and Environmental Engineering, College of Engineering, University of California, Berkeley, CA.

DiPaolo, B.P., Monteiro, P.J.M., Gronsky, R., 2004. Quasi-static axial crush response of a thin-wall, stainless steel box component. International Journal of Solids and Structures 41, 3707–3733.

Empire, 2003. AISI 316 Stainless steel tube – One 20-foot length – 2-inch square × 16-gage wall thickness – Heat number 926594. Empire Metal Supply, Inc., Hauppauge, NY, USA.

Ezra, A.A., Fay, R.J., 1972. An assessment of energy absorbing devices for prospective use in aircraft impact situations. In: Herrmann, G., Perrone, N. (Eds.), Dynamic Response of Structures – Proceedings of a Symposium, June 28 and 29, 1971, Stanford, CA. Pergamon Press, New York, pp. 225–246.

Geoffroy, J.L., Cambien, I., Jouet, A., 1993. Contribution of high strength steels to the absorption of impact energy. La Metallurgia Italiana 85 (6), 377–382.

Gray, R.J., Holbert, R.K., Thrasher, T.H., 1985. Microstructural analysis for series 300 stainless steel sheet welds and tensile samples. In: Northwood, D.O., White, W.E., Vander Voort, G.F. (Eds.), Proceedings of the Sixteenth Annual Technical Meeting of the International Metallographic Society – Corrosion, Microstructure and Metallography, Microstructural Science, vol. 12. ASM International, Materials Park, OH, pp. 345–370.

Griffiths, A.J., Wright, J.C., 1969. Mechanical properties of austenitic and metastable stainless steel sheet and their relationships with pressforming behaviour. In: Stainless Steels – Proceedings of the Conference on Stainless Steels for the Fabricator and User, September 10–12, 1968, Birmingham, UK, 117. Staples Printers Limited for The Iron and Steel Institute, London, pp. 51–65.

Gupta, N.K., Gupta, S.K., 1993. Effect of annealing, size and cut-outs on axial collapse behaviour of circular tubes. International Journal of Mechanical Sciences 35 (7), 597–613.

Hanssen, A.G., Langseth, M., Hopperstad, O.S., 1999. Static crushing of square aluminium extrusions with aluminium foam filler. International Journal of Mechanical Sciences 41, 967–993.

Hecker, S.S., Stout, M.G., Staudhammer, K.P., Smith, J.L., 1982. Effects of strain state and strain rate on deformation – induced transformation in 304 stainless steel: Part I. Magnetic measurements and mechanical behavior. Metallurgical Transactions A 13 (April), 619–626.

Johnson, W., Reid, S.R., 1978. Metallic energy dissipating systems. Applied Mechanics Reviews 31 (3), 277–288.

Johnson, W., Soden, P.D., Al-Hassani, S.T.S., 1977. Inextensional collapse of thin-walled tubes under axial compression. Journal of Strain Analysis 12 (4), 317–330.

Jones, N., 1997. Structural Impact. Cambridge University Press, Cambridge, UK.

Lampinen, B.E., Jeryan, R.A., 1983. Effectiveness of polyurethane foam in energy absorbing structures (820494). Society of Automotive Engineers, Warrendale, PA, pp. 2059–2076.

Langseth, M., Hopperstad, O.S., 1996. Static and dynamic axial crushing of square thin-walled aluminium extrusions. International Journal of Impact Engineering 18 (7–8), 949–968.

Lee, S., Hahn, C., Rhee, M., Oh, J.-E., 1999. Effect of triggering on the energy absorption capacity of axially compressed aluminum tubes. Materials and Design 20, 31–40.

Logan, R.W., Burger, M.J., McMichael, L.D., Parkinson, R.D., 1993. Crashworthiness analysis using advanced material models in Dyna3D. In: Reid, J.D., Yang, K.H. (Eds.), Crashworthiness and Occupant Protection in Transportation Systems 1993 – The 1993 ASME Winter Annual Meeting, November 28–December 3, 1993, New Orleans, LA, AMD169/BED 25. The American Society of Mechanical Engineers, New York, pp. 127–136.

Magee, C.L., Thornton, P.H., 1979. Design Considerations in Energy Absorption by Structural Collapse (780434). Society of Automotive Engineers, Warrendale, PA, pp. 2041–2055.

Mahmood, H.F., Paluszny, A., 1981. Design of thin walled columns for crash energy management – their strength and mode of collapse. In: Proceedings of the Fourth International Conference on Vehicle Structural Mechanics (811302). Society of Automotive Engineers, Warrendale, PA, pp. 7–18.

Mahmood, H.F., Paluszny, A., 1982. Stability of plate-type box columns under crush loading. In: Kamal, M.M., Wolf, J.A. (Eds.), Computational Methods in Ground Transportation Vehicles – The Winter Annual Meeting of the American Society of Mechanical Engineers, November 14–19, 1982, Phoenix, AZ. American Society of Mechanical Engineers, New York, pp. 17–33.

Maldonado, J.G., Advani, A.H., Murr, L.E., Fisher, W.W., 1994. Strain-induced martensite effects on transgranular carbide precipitation and chromium-depletion in austenitic stainless steels. In: Brooks, C.R., Louthan, M.R. (Eds.), Metallographic Investigations of Corrosion, Deformation and Fracture of Engineering Materials – Proceedings of the Twenty-Sixth Annual Technical Meeting of the International Metallographic Society, Microstructural Science, vol. 21. ASM International, Materials Park, Ohio, pp. 23–32.

Mamalis, A.G., Viegelahn, G.L., Manolakos, D.E., Johnson, W., 1986. Experimental investigation into the axial plastic collapse of steel thin-walled grooved tubes. International Journal of Impact Engineering 4 (2), 117–126.

Marshall, N.S., Nurick, G.N., 1998. The effect of induced imperfections on the formation of the first lobe of symmetric progressive buckling of thin-walled square tubes. In: Jones, N., Talaslidis, D.G., Brebbia, C.A., Manolis, G.D. (Eds.), Structures Under Shock and Impact V – SUSI 98. Computational Mechanics Publications, Southampton, UK, pp. 155–168.

McGregor, I.J., Meadows, D.J., Scott, C.E., Seeds, A.D., 1993. Impact performance of aluminium structures. In: Jones, N., Wierzbicki, T. (Eds.), Structural Crashworthiness and Failure. Elsevier Applied Science, London, pp. 385–421 (Chapter 10).

Ohkubo, Y., Akamatsu, T., Shirasawa, K., 1974. Mean Crushing Strength of Closed-Hat Section Members (740040). Society of Automotive Engineers, Warrendale, PA, pp. 223–232.

O'Neal Steel, 2002a. AISI 316/316L Stainless steel tube – Two 20-foot lengths – 2-inch square × 16-gage wall thickness – Heat number 891517. O'Neal Steel/Metals, Inc., Jackson, MS, USA.

O'Neal Steel, 2002b. HREW ASTM A513 Type 1 – Two 20-foot lengths – 2-inch square × 16-gage wall thickness – Item number 872781. O'Neal Steel/Metals, Inc., Jackson, MS, USA.

OnlineMetals, 2002. Carbon ASTM A36 Hot-rolled square tube – Four 96-inch lengths – 2-inch square × 16 gage wall thickness – Part number 10339. OnlineMetals.com, Seattle, WA, USA.

Powell, G.W., Marshall, E.R., Backofen, W.A., 1958. Strain hardening of austenitic stainless steel. Transactions of the American Society for Metals 50, 478–497.

Pugsley, A., 1960. The crumpling of tubular structures under impact conditions. Symposium on the Use of Aluminium in Railway Rolling Stock. The Institution of Locomotive Engineers and the Aluminium Development Association, London, pp. 33–41.

Reid, S.R., Reddy, T.Y., 1986. Axially loaded metal tubes as impact energy absorbers. In: Bevilacqua, L., Feijoo, R., Valid, R. (Eds.), Inelastic Behaviour of Plates and Shells – International Union of Theoretical and Applied Mechanics Symposium, August 5–9, 1985, Rio de Janeiro, Brazil. Springer-Verlag, Berlin, pp. 569–595.

Ryerson, 1991. Ryerson Stock List – Steel, Aluminum, Nickel, Plastics, Copper, Brass – Processing and Fabricating. Joseph T. Ryerson & Son, Inc., Chicago, IL, USA.

Ryerson, 1998. AISI 304 Ornamental Stainless Steel Tube – Four 20-foot lengths – 2-inch square × 16-gage wall thickness – Reference Number 711189. Joseph T. Ryerson & Son, Inc., Chicago, IL, USA.

Santosa, S.P., Wierzbicki, T., Hanssen, A.G., Langseth, M., 2000. Experimental and numerical studies of foam-filled sections. International Journal of Impact Engineering 24, 509–534.

Seitzberger, M., Rammerstorfer, F.G., Gradinger, R., Degischer, H.P., Blaimschein, M., Walch, C., 2000. Experimental studies on the quasi-static axial crushing of steel columns filled with aluminium foam. International Journal of Solids and Structures 37, 4125–4147.

Soden, P.D., Al-Hassani, S.T.S., Johnson, W., 1974. The crumpling of polyvinylchloride tubes under static and dynamic axial loads. Institute of Physics Conference Series No. 21, Oxford, pp. 327–338.

Struers, 2003. 2003 Materialographic Consumables Product Guide. Struers, Inc., Westlake, OH, USA.

Tani, M., Funahashi, A., 1978. Energy absorption by the plastic deformation of body structural members. In: SAE Congress and Exposition, Cobo Hall, February 27–March 3, 1978, Detroit, MI (780368). Society of Automotive Engineers, Warrendale, PA, pp. 1–12.

Thornton, P.H., 1975. Static and dynamic collapse characteristics of scale model corrugated tubular sections. Transactions of the ASME – Journal of Engineering Materials and Technology 75, 357–362.

Thornton, P.H., 1979. Energy absorption by structural collapse in dual phase steel tubes. Metallurgical Transactions A 10 (August), 1199–1201.

Thornton, P.H., Magee, C.L., 1977. The interplay of geometric and materials variables in energy absorption. Transactions of the ASME – Journal of Engineering Materials and Technology 99 Series H (2), 114–120.

Toda, K., Gondoh, H., Takechi, H., Usuda, M., 1976. Absorbed energy during compression and crushing of high strength steel sheets. Metallurgical Transactions A 7 (November), 1637–1642.

VanKuren, R.C., Scott, J.E., 1978. Energy absorption of high-strength steel tubes under impact crush conditions (770213). Society of Automotive Engineers, Warrendale, PA, pp. 947–954.

White, M.D., Jones, N., Abramowicz, W., 1999. A theoretical analysis for the quasi-static axial crushing of top-hat and double-hat thin-walled sections. International Journal of Mechanical Sciences 41, 209–233.

Wierzbicki, T., Abramowicz, W., 1983. On the crushing mechanics of thin-walled structures. Transactions of the ASME – Journal of Applied Mechanics 50 (4a), 727–734.

Wierzbicki, T., Abramowicz, W., 1989. The mechanics of deep plastic collapse of thin-walled structures. In: Wierzbicki, T., Jones, N. (Eds.), Structural Failure. John Wiley, New York, pp. 281–329 (Chapter 9).

Wong, H.F., Rhodes, J., Zaras, J., Ujihashi, S., 1997. Experimental investigation of static progressive crushing of closed-hat section members. In: Gupta, N.K. (Ed.), Plasticity and Impact Mechanics. New Age International Ltd, New Delhi, pp. 250–272.

Yamaguchi, S., Kato, H., Okazaki, T., 1985. Efficient energy absorption of automobile side rails. In: Tenth International Technical Conference on Experimental Safety Vehicles, July 1–4, 1985, Oxford, England. US Department of Transportation, National Highway Traffic Safety Administration, pp. 321–326.

Yamaya, M., Tani, M., 1971. Energy absorption by the plastic deformation of sheet metal columns with box-shaped cross section. Technical Review (June), Mitsubishi Heavy Industries, Ltd., pp. 59–66.